

Article

Enhanced Thermostability of *Pseudomonas nitroreducens* Isoeugenol Monooxygenase by the Combinatorial Strategy of Surface Residue Replacement and Consensus Mutagenesis

Xin-Yi Lu, Xiao-Mei Wu, Bao-Di Ma * and Yi Xu * 

School of Chemical and Environmental Engineering, Shanghai Institute of Technology, Shanghai 201418, China; 186061507@mail.sit.edu.cn (X.-Y.L.); wuxiaomei@sit.edu.cn (X.-M.W.)

* Correspondence: mbd2966@sit.edu.cn (B.-D.M.); xuyi@sit.edu.cn (Y.X.); Tel.: +86-21-60877231 (B.-D.M.); +86-21-60873024 (Y.X.)



Citation: Lu, X.-Y.; Wu, X.-M.; Ma, B.-D.; Xu, Y. Enhanced Thermostability of *Pseudomonas nitroreducens* Isoeugenol Monooxygenase by the Combinatorial Strategy of Surface Residue Replacement and Consensus Mutagenesis. *Catalysts* **2021**, *11*, 1199. <https://doi.org/10.3390/catal11101199>

Academic Editor: Anwar Sunna

Received: 31 August 2021

Accepted: 28 September 2021

Published: 30 September 2021

Publisher's Note: MDPI stays neutral with regard to jurisdictional claims in published maps and institutional affiliations.



Copyright: © 2021 by the authors. Licensee MDPI, Basel, Switzerland. This article is an open access article distributed under the terms and conditions of the Creative Commons Attribution (CC BY) license (<https://creativecommons.org/licenses/by/4.0/>).

Abstract: Vanillin has many applications in industries. Isoeugenol monooxygenase (IEM) can catalyze the oxidation of isoeugenol to vanillin in the presence of oxygen under mild conditions. However, the low thermal stability of IEM limits its practical application in the biosynthesis of natural vanillin. Herein, two rational strategies were combined to improve the thermostability of IEM from *Pseudomonas nitroreducens* Jin1. Two variants (K83R and K95R) with better thermostability and one mutant (G398A) with higher activity were identified from twenty candidates based on the Surface Residue Replacement method. According to the Consensus Mutagenesis method, one mutant (I352R) with better thermostability and another mutant (L273F) with higher activity were also identified from nine candidates. After combinatorial mutation, a triple mutant K83R/K95R/L273F with the best thermostability and catalytic efficiency was generated. Compared with the wild-type IEM, the thermal inactivation half-lives ($t_{1/2}$) of K83R/K95R/L273F at 25 °C, 30 °C, and 35 °C increased 2.9-fold, 11.9-fold, and 24.7-fold, respectively. Simultaneously, it also exhibited a 4.8-fold increase in k_{cat} , leading to a 1.2-fold increase in catalytic efficiency (k_{cat}/K_m). When the whole cell of K83R/K95R/L273F was applied to the biotransformation of isoeugenol on preparative scale, the vanillin concentration reached 240.1 mM with space-time yield of 109.6 g/L/d, and vanillin was achieved in 77.6% isolated yield and >99% purity.

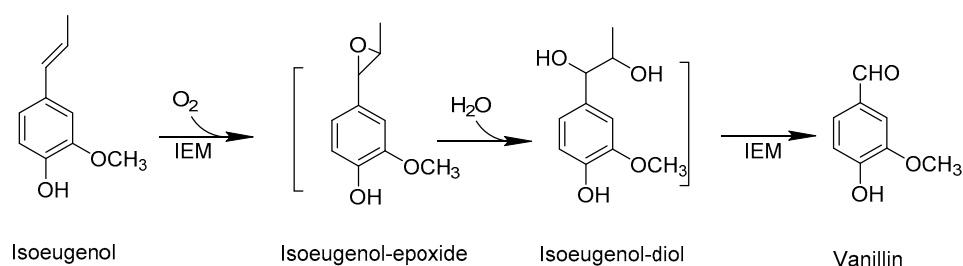
Keywords: vanillin; isoeugenol monooxygenase; thermostability; surface residue replacement; consensus mutagenesis

1. Introduction

Vanillin (4-hydroxy-3-methoxybenzaldehyde, $C_8H_8O_3$), which is a valuable aromatic compound, has many applications in foods, beverages, cosmetics, and pharmaceuticals [1–3]. As the queen of food ingredients, the annual demand for vanillin is as high as 20,000 tons globally [4]. Currently, vanillin is chiefly produced by chemical synthesis [5–7], microbial [8–10]/plant cells [11] and enzymatic biotransformation [12–15]. With the increasing concern for nutrition and health, more and more consumers are inclined to eat natural food additives. Natural vanillin is very expensive and cannot be satisfied only by extracting from vanilla pods (synthetic vanillin: \$15/kg; natural vanillin: \$1200–4000/kg) [16].

Biotechnological production of vanillin is an alternative green approach since its product can be labeled as “natural”. Vanillin production by microorganisms like *Pseudomonas putida* IE27 [8], *Pseudomonas resinovorans* SPR1 [9], *Pediococcus acidilactici* [10], and *Bacillus aryabhattai* BA03 [17] have been extensively studied. However, complex metabolites in microorganisms always lead to the generation of undesired by-products which results in an increased interest in the enzymatic synthesis of vanillin. For example, recombinant *Pediococcus acidilactici* BD16 (fcs^+/ech^+) was confirmed to convert ferulic acid to vanillin through a coenzyme A-dependent pathway [18]. García-Bofill et al. reported an eugenol

oxidase immobilized onto Epoxy-agarose as the biocatalyst for the transformation of vanillyl alcohol to vanillin and finally the space-time yield reached 2.9 g/L/h [19]. Eugenol and isoeugenol are abundant from essential oil and have great potential as the economical precursor for vanillin production [15,20]. Isoeugenol monooxygenase (IEM) is a key enzyme capable of catalyzing the double-bond cleavage of isoeugenol to form vanillin without any cofactors (Scheme 1), such as IEM from *Pseudomonas putida* IE27, *Pseudomonas nitroreducens* Jin1, and metagenomic DNA from soil [12,15,21]. In our previous study, recombinant IEM from *P. nitroreducens* Jin1 was constructed for converting isoeugenol to vanillin, after culture conditions and process optimization, we obtained the maximum enzyme activity of 2050 U/L and 84% conversion to vanillin with the help of magnetic chitosan membrane for in-situ product removal [22]. However, IEMs reported up to now showed relatively low thermostability and enzyme activity which limited its practical application.



Scheme 1. The mechanism of biocatalytic synthesis of vanillin by IEM.

Directed evolution is a useful protein engineering method [23], and numerous researches enhanced enzymes' performances at elevated temperatures by employing error-prone PCR [24,25]. However, it is very time-consuming to screen large mutant pools, especially for those enzymes without efficient high-throughput screening approaches. In recent years, emerging rational strategies are developed more efficient in the improvements of protein thermostability with the aid of computational tools, such as disulfide bridges introduction [26], consensus mutagenesis [27–29] and $\Delta\Delta G$ calculation by FoldX [30].

According to the evolutionary information of thermophilic bacteria, glycine and lysine on the surface of thermophilic proteins were replaced by alanine and arginine, respectively [31]. Generally speaking, the proteins' thermal stability was related to the composition of surface amino acids, and the effect of alanine and arginine was to increase internal hydrophobicity and to favor helix stabilizing residues [31,32]. Liu et al. modified the thermostability of cysteine sulfinic acid decarboxylase by surface residue replacement (Gly \rightarrow Ala, Lys \rightarrow Arg) and obtained a mutant G369A in which the optimal temperature was increased 2 °C [33]. Consensus mutagenesis is an approach to identify conserved amino acid residues by aligning a series of homologous sequences because conserved amino acids are more helpful for protein folding stability than those non-conserved amino acids [34]. The mutant T383K of glutamate decarboxylase from *Lactobacillus Brevis* and variant H210N/I77L/M150C-M280C of (*R*)-selective amine transaminase from *Aspergillus terreus* had a large shift in thermostability by using Consensus Finder, with an almost 1.7-fold increase in $t_{1/2}$ at 55 °C and 16.6-fold increase in $t_{1/2}$ at 40 °C, respectively [28,29]. Combining different strategies had been proven to further improve the thermostability of enzymes [35,36], such as the combination of B-factor analysis and multiple sequence alignment [37].

The purpose of this work was to enhance the thermostability of IEM from *P. nitroreducens* Jin1 by combining the strategies of surface residue replacement and consensus mutagenesis for the first time. The GETAREA (<http://curie.utmb.edu/getarea.html>) [38] and Consensus Finder (<http://kazlab.umn.edu/>) [39] online server were used to predict stabilizing substitutions in IEM. The positive single-site mutants were selected from the predict candidate mutants based on experimental verification. Subsequently, the positive mutations were combined together to obtain the multi-site mutants with higher thermostability of IEM. The positive variants were characterized and compared with the wild-type. Subse-

quently, the synthesis of natural vanillin was conducted by the best mutant of IEM. And the potential reasons contributing to the improvement of thermostability were also discussed.

2. Results

2.1. Selection of Sites for Surface Residue Replacement and Consensus Mutagenesis

Replacing surface glycine and lysine with alanine and arginine was considered as an effective approach to enhance proteins' thermal stability [31–33]. The 3D structure of IEM was submitted to GETAREA and six glycines and fourteen lysines on the surface were chosen for mutation (Figure 1a). All of them were far away from the active center so that the substitutions might have little impact on the enzyme activity.

Consensus Finder is an open-source website that can predict the potential stable amino acid replacements based on consensus mutagenesis. After aligning 68 homologous sequences of IEM, nine mutants (V130L, S182Y, L303N, I352R, D176E, N312G, F216M, L273F, E47D) were selected and all the consensus residue had a threshold above 70%. As shown in Figure 1b, V130, D176, L273 were buried at the β -sheet, while S182, L303, I352, N312, F216, E47 lied on the loop regions.

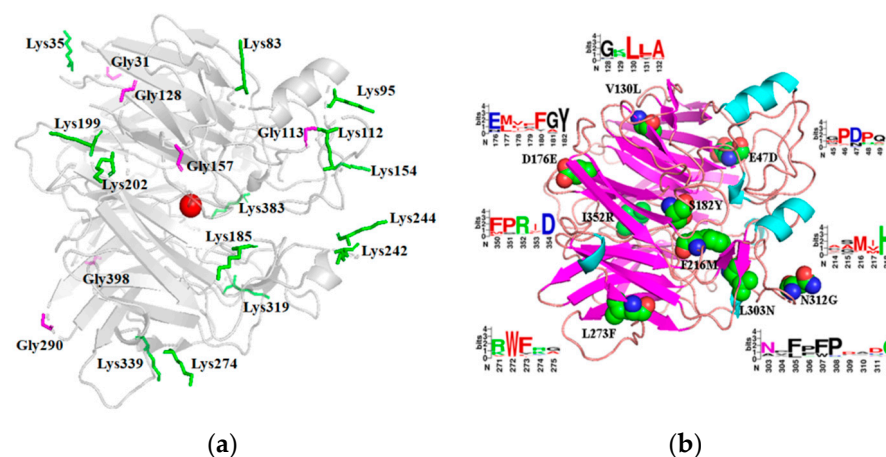


Figure 1. The distribution of mutated residues in the three-dimensional structure of IEM. (a) Glycines and lysines on the surface of IEM, predicted by GETAREA. Green represents lysine and purple represents glycine. (b) Locations of nine mutations identified by consensus analysis. Mutated sites are designated by spheres and frequencies of replacement residues are shown as a logo by WebLogo. The height of letters stands for the frequency of each amino acid in the corresponding position.

2.2. Preliminary Selection of IEM Mutants with Improved Thermostability and Activity

29 variants selected by GETAREA and Consensus Finder were constructed by using the whole plasmid PCR technique (See Section 4.2 for details). The crude enzymes were incubated at 35 °C for 15 min and the residual activities of mutants were compared with wild-type IEM. As shown in Table 1, two variants (K83R, K95R) exhibited better thermostability based on the strategy of Surface Residue Replacement which kept 84.2% and 68.0% of initial activity, respectively, while the wild-type IEM lost nearly 50% activity. Additionally, a positive mutant G398A resulted in a 1.3-fold increase in specific activity was obtained. Meanwhile, nine variants were constructed to match the strategy of Consensus Mutagenesis by discarding those with a low conservation threshold. The results showed that I352R might improve thermostability (70.4% residual activity) and L273F exhibited an almost 1.2-fold increase in specific activity. Other variants that processed a slight increase of thermal stability (K112R, K244R, K274R, and N312G) or even reduced thermal stability (the remaining 20 mutants) were removed. Details were shown in Table S1.

Five of the predicted 29 variants were regarded as the most promising candidates, and they were combined together for further improvement of the thermostability and enzyme activity. Then, the combinatorial variants (K83R/K95R, K83R/I352R, K83R/K95R/I352R, K83R/K95R/G398A, and K83R/K95R/L273F) were generated with notably improved

thermostability. Subsequently, the most thermostable mutant K83R/K95R/L273F which showed enhanced thermostability with <2% IEM activity loss was chosen and subjected to further experiments.

Table 1. Comparison of the enzyme activity and residual activity between IEM and its positive mutants.

Strategy	Mutants	Relative Activity (%) [#]	Residual Activity (%) [*]
-	IEM	100.0 ± 8.0	53.2 ± 2.4
	K83R	103.9 ± 3.8	84.2 ± 2.7
	K95R	106.6 ± 3.7	68.0 ± 0.4
	G398A	130.4 ± 1.5	55.6 ± 1.5
Surface residue replacement	I352R	99.7 ± 1.3	70.4 ± 2.4
	L273F	117.2 ± 0.6	50.4 ± 0.6
	K83R/K95R	104.8 ± 1.0	92.1 ± 0.9
Consensus mutagenesis	K83R/I352R	99.2 ± 4.2	87.8 ± 3.0
	K83R/K95R/I352R	114.3 ± 2.1	90.1 ± 2.5
Combinatorial mutagenesis	K83R/K95R/G398A	130.1 ± 3.0	94.1 ± 1.5
	K83R/K95R/L273F	168.2 ± 7.3	98.5 ± 0.3

[#] The enzyme activity was assayed at 30 °C and pH 8.0 (0.1 M Tris-HCl) for 10 min and the activity of wild-type IEM was set as 100%. ^{*} The residual activities of crude enzymes were determined after heat-treatment at 35 °C for 15 min and the initial activity of each mutant was defined as 100%, respectively.

2.3. Thermostability and Kinetic Analysis of IEM and Its Mutants

According to the screening results, five mutants in total (K83R, K95R, L273F, K83R/K95R, K83R/K95R/L273F) were selected for comparing the half-lives ($t_{1/2}$) with the wild-type IEM. The SDS-PAGE of the purified IEM and its mutants were displayed in Figure S1. The purified enzymes were incubated at 25 °C, 30 °C, and 35 °C for different times. The $t_{1/2}$ value of the wild-type IEM was 7.8 min at 35 °C while K83R, K95R, L273F, K83R/K95R, and K83R/K95R/L273F mutant enzymes were 31.8 min, 28.8 min, 12.6 min, 94.8 min, and 192.6 min, respectively, corresponding to 4.1-, 3.7-, 1.6-, 12.0- and 24.7-fold higher than that of IEM (Table 2). For thermal stability, the best-performing mutant was K83R/K95R/L273F.

Table 2. Half-lives of IEM and its mutants for thermal inactivation.

Enzymes [*]	$t_{1/2}$		
	25 °C (min)	30 °C (min)	35 °C (min)
Wild-type	967.2	49.8	7.8
K83R	1094.4	267.2	31.8
K95R	1108.8	198.0	28.8
L273F	602.7	133.2	12.6
K83R/K95R	2224.2	491.4	94.8
K83R/K95R/L273F	2848.8	594.0	192.6

^{*} The enzyme activity was assayed at pH 8.0 (0.1 M Tris-HCl) and 30 °C for 10 min. For details, please see experimental Section 4.5.

Kinetic constants of the enzymes were determined by using isoeugenol as a substrate at 30 °C and pH 8.0. The results summarized in Table 3 showed that all variants increased enzyme activity due to the increased k_{cat} which was the major factor affecting the reaction rate. Among them, mutant K83R/K95R/L273F showed a 4.8-fold increased k_{cat} value, leading to a 1.2-fold increase in catalytic efficiency (k_{cat}/K_m). However, all variants had higher K_m values, indicating that substrate affinity might be reduced. Additionally, K83R/K95R/L273F also demonstrated excellent thermostability over 25 °C to 35 °C, as discussed above (Table 2). Enzymes with high catalytic efficiency and high stability are attractive candidates for industrial production. Consequently, favorable enzymatic properties make K83R/K95R/L273F more appropriate in potential industrial applications.

Table 3. Kinetic parameters and specific activity of IEM and its mutants.

Enzymes	K_m (mM)	k_{cat} (s^{-1})	k_{cat}/K_m ($mM^{-1} s^{-1}$)	Specific Activity * ($U\ mg^{-1}$)
Wild-type	0.1 ± 0.02	2.1 ± 0.09	21.0	3.4 ± 0.15
K83R	0.6 ± 0.12	5.5 ± 0.41	9.2	6.1 ± 0.04
K95R	0.4 ± 0.12	6.1 ± 0.55	15.3	5.3 ± 0.02
L273F	0.3 ± 0.11	6.9 ± 0.49	23.0	5.5 ± 0.09
K83R/K95R	0.5 ± 0.11	10.5 ± 0.69	21.0	6.0 ± 0.14
K83R/K95R/L273F	0.4 ± 0.12	10.1 ± 0.92	25.3	7.0 ± 0.04

* The specific activity was assayed at pH 8.0 (0.1 M Tris-HCl) and 30 °C for 10 min with substrate concentration of 10 mM. For details, please see experimental Section 4.4.

2.4. Enzymatic Properties of IEM and Its Mutant IEM^{K83R/K95R/L273F}

The enzymatic properties of the purified IEM and mutant K83R/K95R/L273F were investigated. Similar to IEM from *P. putida* IE27 [20], both IEM and its mutant demonstrated optimal temperatures of 30 °C (Figure 2a). In Figure 2b, the variant K83R/K95R/L273F showed higher thermal stability between 30 °C to 35 °C and remained above 80% activities at 35 °C, while the wild-type IEM only maintained 34.5% activity. However, both of them were completely inactivated after incubation at 40 °C for 30 min, which might be due to the structure of protein destroyed at higher temperatures.

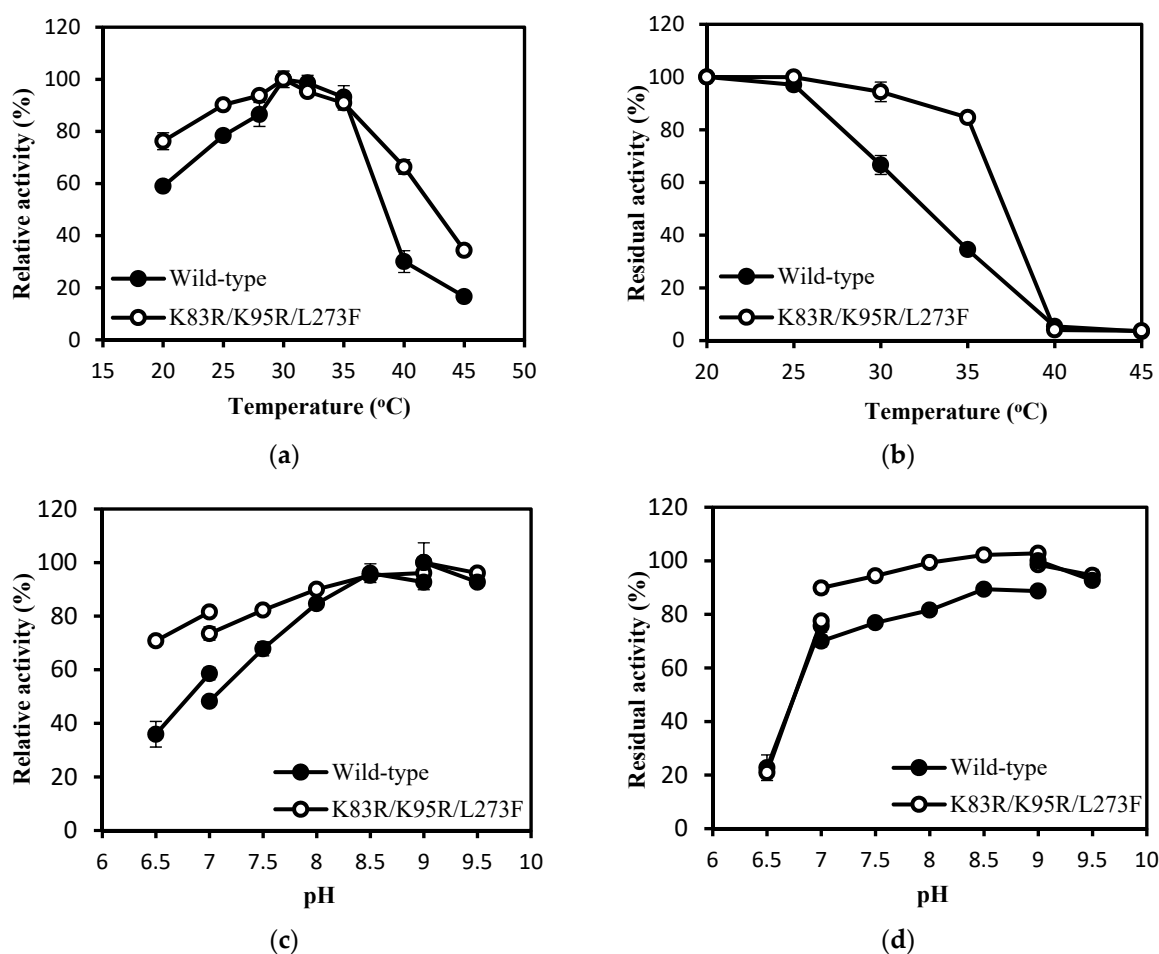


Figure 2. Characterization of IEM and its variant K83R/K95R/L273F. (a) Effect of temperature on the activity of wild-type IEM and K83R/K95R/L273F. The reaction was carried at various temperatures (20 °C to 45 °C) in Tris-HCl (100 mM, pH 8.0). The highest activities of the wild-type IEM (3.4 U/mg) and K83R/K95R/L273F (7.0 U/mg) were defined as 100%, respectively. (b) The thermostability of wild-type IEM and K83R/K95R/L273F. The thermostability was measured by monitoring the residual activity after incubation at different temperatures (20 °C to 45 °C) for 30 min. The respective initial

activity was defined as 100%. (c) Effect of pH on the activity of wild-type IEM and K83R/K95R/L273F. The reaction was conducted at 30 °C using the following buffers (pH 6.5~7.0 PB buffer; pH 7.0~9.0 Tris-HCl buffer; pH 9.0~9.5 Gly-NaOH buffer). The relative activity was expressed as a percentage of each activity to their respective maximum activity. (d) The pH stability of wild-type IEM and K83R/K95R/L273F. The pH stability was measured by monitoring the residual activity after incubation in various buffers at 4 °C for 18 h. The respective initial activity at different pH was defined as 100%.

The optimum pH of IEM and K83R/K95R/L273F were 9.0 (Figure 2c). The relative activities of K83R/K95R/L273F were higher than IEM at pH 6.5~8.0. The mutant retained $\geq 70\%$ activity between 6.5 to 9.5, but IEM remained 70% relative activity in a narrower pH range from 8.0 to 9.5, indicating that the mutant performed increased preference of neutral environments. Of note, K83R/K95R/L273F was also more stable than IEM under pH conditions of 7.0~8.5 (Figure 2d).

All metal ions had a negative impact on the enzyme activity of IEM, especially Zn^{2+} and Ni^{2+} (Figure S2a). In comparison with the wild-type IEM, the tolerance of K83R/K95R/L273F to metal ions was also improved. Aside from Zn^{2+} , other metal ions with low concentrations didn't have too much inhibitory effect on the activity of K83R/K95R/L273F (Figure S2b). When 10 mM Mn^{2+} , Ca^{2+} , and Fe^{3+} were added to the reaction system, the activity of K83R/K95R/L273F could remain at 80.4%, 78.2%, and 73.7%, respectively, whereas the wild-type remained at only 69.4%, 64.6%, and 21.6%. In addition, the mutant did not overcome the problem of product inhibition. Figure S3 showed that an incremental decrease in activities of the wild-type and K83R/K95R/L273F was noticeable with the increasing vanillin concentration.

2.5. Biocatalytic Synthesis of Vanillin by IEM and Its Mutant IEM^{K83R/K95R/L273F}

The catalytic efficiency of K83R/K95R/L273F was 1.2-fold higher than IEM, revealing that K83R/K95R/L273F was a positive mutation that might be favorable to the production of vanillin. To evaluate the effect of mutation of IEM on vanillin biosynthesis, both wild-type and K83R/K95R/L273F were used to convert isoeugenol into vanillin at different temperatures and pH for 8 h. The conversion of isoeugenol for K83R/K95R/L273F increased from 20 °C to 35 °C, and reached the maximum (82.5%) at 35 °C. However, the conversion of isoeugenol for wild-type IEM sharply decreased when the temperatures were beyond 30 °C and the conversion was only 54.5% at 35 °C (Figure 3a), which might due to the fact that the native IEM had poor thermal stability on higher temperature and it quickly lost its activity at 35 °C. Furthermore, the conversion of isoeugenol achieved with K83R/K95R/L273F was higher than those obtained from wild-type IEM at pH 7.0~9.0 (Figure 3b). The results indicated that K83R/K95R/L273F exhibited better performance than wild IEM at test temperature and pH range.

Based on the reaction conditions of our previous report [22], the scale-up of natural vanillin was completed in a 250 mL conical flask using the *E. coli* cells harboring variant K83R/K95R/L273F. Chitosan membrane was added into biotransformation system for in-situ product isolation due to Schiff base formation between chitosan and vanillin. The amino group in the chitosan membrane reacted with the aldehyde group of vanillin to form a Schiff base so that vanillin could be removed from the reaction solution in time. Under the optimal conditions (30 °C, pH 9.0, 180 rpm, 15 g/L cells, 1.2 g chitosan membrane), the yield of vanillin reached 240.1 mM (36.5 g/L) after 8 h reactions with 300 mM isoeugenol (49.2 g/L), and the conversion was up to 80.0% with the space-time yield of 109.6 g/L/d (>100 g/L/d). The process efficiency had met the basic requirements of industrial biotransformation. And 1.062 g vanillin was obtained after the isolation and purification process with 77.6% isolation yield. The purified product was a pale yellow crystal (Figure S4a) with the HPLC purity of >99% (Figure S4b). The chemical structure of product was verified by ¹H NMR spectrum (Figure S4c).

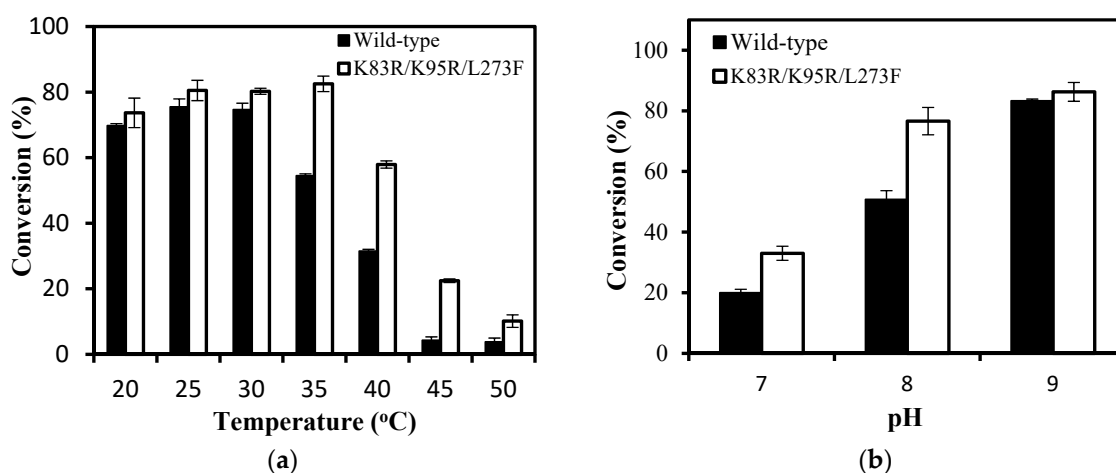


Figure 3. Biotransformation of isoeugenol to vanillin by whole-cells of recombinant IEM and IEM^{K83R/K95R/L273F} at different temperature (a) and pH (b) ranges using isoeugenol as a substrate. (a) The reaction was conducted in Gly-NaOH (0.1 M, pH 9.0) at 20–50 °C for 8 h. (b) The reaction was conducted at 30 °C in Tris-HCl (0.1 M, pH 7.0–9.0) for 8 h. For details, please see experimental Section 4.7. Values are means \pm standard deviation of three replicates (\pm SE).

3. Discussion

Isoeugenol monooxygenase (IEM) from *P. nitroreducens* Jin1 exhibits good performance in the production of natural vanillin but poor thermal stability with a $t_{1/2}$ at 35 °C of merely 7.8 min. Typically, the vital factor that limits enzymes' industrial application is low thermostability. Thus, taking advantage of protein engineering strategies to obtain IEM variants that stay active under moderate conditions for a longer time is very necessary. In this study, a simple but effective combinatorial strategy was successfully applied in improving the thermostability of IEM.

Based on the Surface Residue Replacement (Gly \rightarrow Ala, Lys \rightarrow Arg) and Consensus Mutagenesis [28,29,33], five mutants K83R, K95R, G398A, I352R, and L273F were determined as positive candidates (Table 1). To investigate the possibility of synergistic effect, five combinatorial variants were generated to observe whether thermostability could be further improved [35–37]. K83R, which exhibited the highest stability among 29 single-site mutants, was used as a template for the next combinatorial mutation. We firstly performed combined mutations on the mutants with improved thermostability, including K83R/K95R, K83R/I352R, and K83R/K95R/I352R. It was notable that the thermostability of K83R/K95R/I352R seems comparable to that of K83R/K95R (Figure 4), which showed that the optimal mutant was not always the one with all the beneficial substitutions. Then, the K83R/K95R mutation was introduced into G398A and L273F for increasing the enzyme activity simultaneously, and the variant K83R/K95R/L273F showed the highest activity (Table 1). Additionally, it also had the greatest change in thermostability, with $t_{1/2}$ increased by a 24.7-fold at 35 °C (Table 2).

The modeled structure of IEM showed that K83, K95, and L273 were all located on the protein surface (Figure 5a), which was consistent with the opinion that irreversible thermal denaturation of a protein usually contained an unfolding step and such process primarily involved surface-located regions [40]. Intramolecular interactions including hydrogen bonds, salt bridges, and disulfide bonds had pivotal roles in enhancing the thermal stability of proteins [25,26,28]. When the distance between two polar non-hydrogen atoms was less than 3.5 Å, a hydrogen bond which contributed 0.6 kcal/mol energy to protein stability could be formed [41]. It was clear in Figure 5b that there was a hydrogen bond between the N atom of Lys83/Arg83 and the O atom of Thr149 (2.9 Å), in addition, the N atom of Arg83 also resulted in an additional hydrogen bond with the O atom of Trp81 (3.2 Å). What's more, a cation- π interaction between Arg83 and Phe87 (6.4 Å) was also found, which was a force generated between a cation and an aromatic ring. The energy of cation- π interaction was

2-fold higher than that of the salt bridge and very common in thermophilic bacteria [42], so K83R showed the highest thermostability among all single-point mutations. Similarly, the N atom of Lys95/Arg95 formed one hydrogen bond with the O atom of Glu90 (3.2 Å), when Lys95 was replaced by Arg95, a new hydrogen bond was generated with the O atom of Gln53 (3.5 Å) (Figure 5c). This suggested that K95R mutation might enhance IEM's thermal stability by the additional hydrogen bond. Arginine could reach further in space due to its longer side chain so that the additional hydrogen bond interactions probably occurred as a consequence [32]. The temperature factors (B-factors) reflect atomic flexibility and protein dynamics of crystal structure, proposing that larger B-factor value indicate higher flexibility [37]. And the B-factor values of K83R and K95R decreased from 0.80 to 0.76 and 0.70 to 0.64, respectively, indicating that protein was more stable after mutation.

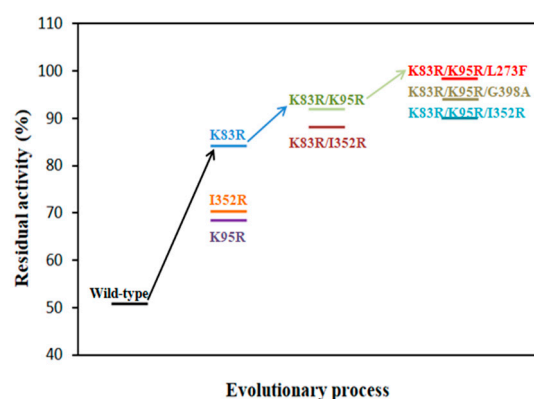


Figure 4. The evolutionary process of IEM for improving its thermostability. The residual activities of IEM and variants were determined after heat-treatment at 35 °C for 15 min. The respective initial activity was taken as 100%. The enzyme activity was assayed at 30 °C and pH 8.0 (0.1 M Tris-HCl) for 10 min.

The $t_{1/2}$ at 30 °C of double-site mutant K83R/K95R increased by 1.9- and 2.5-fold compared to K83R and K95R respectively, which indicated that K83R and K95R might have an unexpected additive effect. As illustrated in Figure 5d, the Arg83 and Arg95 residues were located at loop regions from the C-terminal and N-terminal of α -helix, and the combined effects of increased hydrogen bonds and cation- π interaction might further reinforce the conformational rigidity of this local region.

As for the mutation L273F, whose main contribution was to enhance the enzyme activity, was buried in a β -sheet region and this residue was replaced by aromatic phenylalanine with no change in intra-molecular interactions, both Leu273 and Phe273 had two hydrogen bonds with Ile258 (Figure 5e). We compared the free energy change value (DDG, the unfolding Gibbs free energy value of the mutated protein minus the unfolding Gibbs free energy value of the wild type) of L273F with the wild-type using online software I-mutant 2.0 (<https://folding.biofold.org/i-mutant/i-mutant2.0.html>) [43], DDG positive value of L273F (0.11 kcal/mol) implied that the interaction between position 273 and surrounding amino acids might be enhanced after mutation. Through combining L273F with K83R/K95R, the local area and the whole structure of K83R/K95R/L273F might be stabilized (Figure 5f).

Furthermore, the k_{cat} value of K83R/K95R/L273F was higher than those determined in other studies [15,20] and the k_{cat}/K_m value was 1.2-fold higher than the wild-type, which indicates that it exhibited superior performance both in the thermostability and catalytic efficiency. In general, it was rare to increase the thermal stability of an enzyme without sacrificing catalytic activity [44]. In the previous studies, the biotransformation of isoeugenol to vanillin by IEM was mainly conducted at 20 °C [12,22], while K83R/K95R/L273F could efficiently catalyze such reaction with the highest conversion at 30 °C [15,45,46]. For this bioconversion route, the cost of the enzyme was acceptable, with enzyme activity and stability guaranteed. To meet the requirements of the green industry, enzymatic synthesis

of vanillin had advantages of mild reaction conditions and was environmentally friendly. What's more, isoeugenol was an economically viable precursor for vanillin production at a market price of about \$9/kg [21,47] that made this process more competitive in the synthesis of natural vanillin.

In summary, protein engineering had been more concentrated on improving IEM activity, but few on thermostability [15]. This study emphasized that the 83 position and the loop region around this residue might be critical to IEM's thermostability and these results would provide useful information for molecular modification of IEM in the future. What's more, the conjunction of Surface Residue Replacement and Consensus Mutagenesis would be a more effective and time-saving strategy to improve the thermal stability of IEM, which might be also useful to other enzymes.

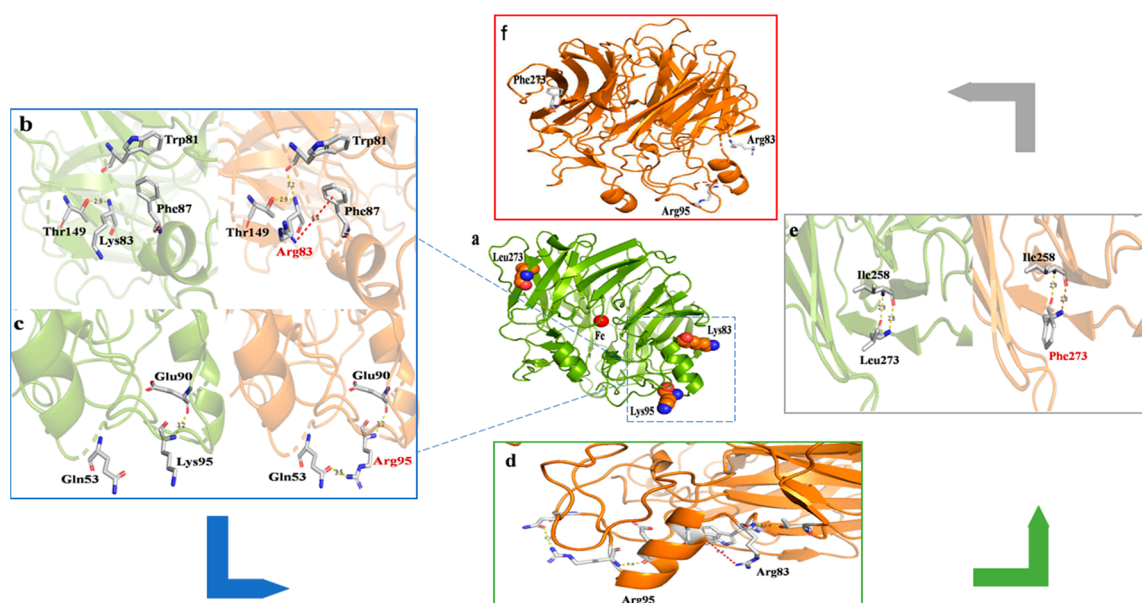


Figure 5. The 3D structure model of IEM (green) and its mutants (orange). (a) wild-type IEM; (b) mutant K83R; (c) mutant K95R; (d) mutant K83R/K95R; (e) mutant L273F; (f) mutant K83R/K95R/L273F.

4. Materials and Methods

4.1. Chemicals, Plasmids and Strains

All chemicals were of the analytical grade commercially available in this study. PrimeSTAR[®] Max DNA polymerase and *Dpn* I was purchased from Takara Biotechnology (Dalian, China). Universal DNA Purification Kit, TIANpure Mini Plasmid Kit, and DNA marker (500–7000 bp) were purchased from Tiangen Biotech Co., Ltd. (Beijing, China). Regular range protein marker (15–130 KDa) was obtained from Sangon Biotech Co., Ltd. (Shanghai, China). *E. coli* BL21(DE3) was utilized as a host for heterologous expression. The recombinant plasmid pET21a-IEM was constructed in our previous work [22].

4.2. Prediction of Potential Stable Variants and Site-Directed Mutagenesis

Homology modeling of IEM was carried out by SWISS-MODEL (<https://swissmodel.expasy.org/>) [48] based on the crystal structure of lignostilbene- α , β -dioxygenase from *Pseudomonas brassicacearum* (PDB ID: 5V2D) with a sequence identity of 42.58% [49]. Then the modeled structure was uploaded to the GETAREA website (<http://curie.utmb.edu/getarea.html>) [38] for predicting surface amino acids. All glycine and lysine residues on the surface were replaced by alanine and arginine, respectively. The quality of modeled structure was validated by PDBsum (<http://www.ebi.ac.uk/thornton-srv/databases/pdbsum>) [50] and VERIFY 3D (<https://servicesn.mbi.ucla.edu/Verify3D/>) [51] (Figure S5).

The protein sequence in FASTA form (Genbank: ACP17973.1) as input to the Consensus Finder (<http://kazlab.umn.edu/>) [39] to find homologous sequences and aligned by Clustal X (Version 2.0, University college Dublin, Dublin, Leinster., Ireland, 2010) [52]. Nine putative mutation sites with the conservation threshold of >70% were chosen for site-directed mutation. The frequency of each amino acid was visualized by WebLogo (<https://weblogo.berkeley.edu/logo.cgi>) [53].

The plasmid pET21a-IEM was used as the template to construct the mutants using the whole plasmid PCR technique [54]. A typical PCR mixture (50 μ L) consisted of 2 \times PrimeSTAR[®] Max DNA polymerase (25 μ L), forward and reverse primers (1 μ L, 10 μ M), plasmid DNA (pET21a-IEM, 1 μ L), and sterile water (22 μ L). The reaction program was as follows: 1 cycle of 10 min at 95 $^{\circ}$ C, 24 cycles of 10 s at 98 $^{\circ}$ C, 15 s at 56 $^{\circ}$ C, 75 s at 72 $^{\circ}$ C, and 1 cycle of 5 min at 72 $^{\circ}$ C. The PCR products were digested for 4 h at 37 $^{\circ}$ C with *Dpn* I, then transformed into *E. coli* BL21 (DE3) and cultured overnight on Luria-Bertani plates with Ampicillin. The sequence of transformants was confirmed by DNA sequencing. Primers were synthesized by BGI (Beijing, China) and listed in Table S2.

4.3. Enzyme Expression and Purification

The optimized fermentation medium and cultivation method for IEM expression was previously described [22]. The recombinant IEM and its variants were purified from the cell lysates using BeaverBeads[™] His-tag Protein Purification (BEAVER Biomedical Engineering Co., Ltd., Suzhou, China) according to the manufacturer's instructions. Specifically, cells were harvested and suspended in binding buffer (20 mM NaH₂PO₄, 500 mM NaCl, 10 mM imidazole, pH 7.4) and were sonicated on ice. The target proteins with His-tag were adsorbed on the magnetic beads, and then IEM and its variants were eluted by using elution buffer (20 mM NaH₂PO₄, 500 mM NaCl, 500 mM imidazole, pH 7.4). The imidazole was eliminated by ultrafiltration using a 10 KDa cut-off membrane (EMD Millipore, Billerica, MA, USA) against Tris-HCl buffer (100 mM, pH 8.0). The purity of the protein was analyzed by 12% SDS-PAGE and protein concentration was determined by the Bradford method [55] with bovine serum albumin as the standard.

4.4. Enzyme Activity Assay and Kinetic Analysis

The reaction system consisting of 100 mM Tris-HCl buffer (pH 8.0), 10 mM isoeugenol, 5% ethanol (*v/v*), and appropriately diluted enzyme solution was incubated at 30 $^{\circ}$ C for 10 min. The reaction was terminated by the addition of 1 mL anhydrous methanol. The concentration of vanillin in samples was analyzed by HPLC [22]. One unit (U) of IEM activity was defined as the amount of enzyme that produced 1 μ mol of vanillin per minute under standard conditions (pH 8.0, 30 $^{\circ}$ C). The enzyme activities were measured at isoeugenol concentrations of 0.05–10 mM to determine the kinetic parameters. Kinetic values were estimated by fitting the Michaelis-Menten plot using non-linear regression with GraphPad Prism software (Version 8.0, GraphPad Software Inc., San Diego, CA, USA, 1995).

4.5. Thermal Stability Assay

The thermal stability of the enzyme was investigated by determining the half-life ($t_{1/2}$) of IEM at various temperatures. The purified wild-type enzyme and mutants (0.7 mg/mL) were incubated at 25 $^{\circ}$ C, 30 $^{\circ}$ C, and 35 $^{\circ}$ C for different times. After defined time intervals, samples were removed and immediately placed on ice for 5 min, then the residual enzyme activity was measured as described above. The first-order inactivation rate constants (k_d) were estimated by linear regression the $\ln(\text{residual activity})$ versus incubation time, and $t_{1/2} = \ln 2/k_d$.

4.6. Effects of Temperature, pH, Metal Ions and Product-Inhibition on Enzyme Activity

To determine the optimum temperature, enzyme activity was assayed in Tris-HCl buffer (100 mM, pH 8.0) between 20 $^{\circ}$ C to 45 $^{\circ}$ C. The relative activity referred to the ratio of the enzyme activity at different temperatures to their respective highest activity (wild-type:

3.4 U/mg, K83R/K95R/L273F: 7.0 U/mg). In terms of thermal inactivation, the purified enzyme (0.7 mg/mL) was assayed by monitoring the residual activity after incubation at 20–45 °C for 30 min. The residual activity was obtained by the ratio of the remaining activity after incubation to the respective initial activity. Experiments were independently performed in triplicate.

To determine the optimum pH, the reactions were carried out at 30 °C in various buffers over a pH range of 6.0–9.5. The relative activity was expressed as a percentage of their respective maximum activity. The pH stability was analyzed by measuring the residual activity after incubation at 4 °C for 18 h in the corresponding buffers and the initial activity of wild-type IEM and K83R/K95R/L273F was defined as 100%, respectively. The average of three independent determinations was shown.

The effects of metal ions on enzyme activity were measured in Tris-HCl buffer (100 mM, pH 8.0) containing different metal ions at a concentration of 1 mM and 10 mM (K^+ , Mg^{2+} , Zn^{2+} , Mn^{2+} , Ca^{2+} , Co^{2+} , Ni^{2+} , Fe^{3+}) at 30 °C. The enzyme activity without any metal ions was used as a control and was set as 100%. Experiments were independently performed in triplicate.

The product-inhibition was detected by adding 0–5 mM vanillin when measuring enzyme activity. The enzyme activity without vanillin was set as 100%. Experiments were independently performed in triplicate.

4.7. Biosynthesis of Vanillin Using Whole-Cell Catalysis

The reactions were carried out in 50 mL conical flasks containing 5 mL reaction volume. The recombinant *E. coli* cells (15 g/L) overexpressing IEM or IEM^{K83R/K95R/L273F} were suspended in various buffers, and then isoeugenol dissolved in 10% DMSO (*v/v*) was added into the reaction system, giving a final substrate conversion of 100 mM. To determine the effect of temperature on the vanillin synthesis, the reaction was conducted at temperatures ranging from 20 °C to 50 °C in Gly-NaOH (100 mM, pH 9.0) for 8 h. To investigate the effect of pH on the vanillin synthesis, the reaction was conducted at 30 °C in Tris-HCl buffer (100 mM, pH 7.0–9.0) for 8 h. Samples were withdrawn to detect the concentration of product by HPLC [22].

4.8. Preparation of Natural Vanillin

The reaction mixture contained 300 mM isoeugenol, 100 mM Gly-NaOH buffer (pH 9.0), 10% DMSO, 1.2 g chitosan membrane, and cells of *E. coli*/pET21a-IEM^{K83R/K95R/L273F}. The reaction was carried out at 30 °C, 180 rpm for 8 h in a total volume of 30 mL, started by adding isoeugenol, and stopped by the addition of 30 mL methanol. After centrifugation, the supernatant was collected and analyzed by HPLC. The chitosan membranes dissolved in 6% hydrochloric acid solution at 30 °C for 12 h. The reaction supernatant and hydrochloric acid solution were combined and filtrated. The filtration was extracted with ethyl acetate and the organic phase was evaporated to obtain crude vanillin. Then the crude product was recrystallized three times with water, and the purified vanillin was verified by HPLC [22] and ¹H NMR (400 MHz, CDCl₃) δ /ppm: 9.83 (s, 1H), 7.43 (d, *J* = 6.4 Hz, 2H), 7.05 (d, *J* = 8.3 Hz, 1H), 6.33 (s, 1H), 3.97 (s, 3H). The chitosan membranes were prepared as previously reported [22].

Supplementary Materials: The following are available online at <https://www.mdpi.com/article/10.3390/catal11101199/s1>, Figure S1: SDS-PAGE assay of purified IEM and its mutants, Figure S2: The effects of mental ions on IEM and K83R/K95R/L273F activities, Figure S3: The effects of product-inhibition on IEM and K83R/K95R/L273F activities, Figure S4: Preparation of natural vanillin, Figure S5: The 3D structure of IEM based on Homology Modeling and qualified by Ramachandran plot, Table S1: The comparison of the enzyme activity and residual activity after 35 °C heat-treatment between IEM and mutants, Table S2: Primers for site-directed mutagenesis.

Author Contributions: Conceptualization, B.-D.M. and Y.X.; methodology, B.-D.M. and Y.X.; validation, X.-Y.L.; formal analysis, X.-Y.L.; data curation, X.-Y.L.; writing—original draft preparation,

X.-Y.L.; writing—review and editing, X.-M.W., B.-D.M. and Y.X.; funding acquisition, B.-D.M. and Y.X. All authors have read and agreed to the published version of the manuscript.

Funding: This research was funded by Open Project Funding of the State Key Laboratory of Biocatalysis and Enzyme Engineering (Grant No. SKLBEE2018008), Shanghai Collaborative Innovation Center of Fragrance Flavor and Cosmetics (Grant No. 1021ZK170004002), Project of Leading Talents in Shandong Taishan Industry (Grant No. LJNY202019).

Data Availability Statement: Data are contained within the article.

Conflicts of Interest: The authors declare no conflict of interest.

References

1. Priefert, H.; Rabenhorst, J.; Steinbüchel, A. Biotechnological production of vanillin. *Appl. Microbiol. Biotechnol.* **2001**, *56*, 296–314. [[CrossRef](#)] [[PubMed](#)]
2. Converti, A.; Aliakbarian, B.; Domínguez, J.M.; BustosVázquez, G.; Perego, P. Microbial production of biovanillin. *Braz. J. Microbiol.* **2010**, *41*, 519–530. [[CrossRef](#)]
3. Sainsbury, P.D.; Hardiman, E.M.; Ahmad, M.; Otani, H.; Seghezzi, N.; Eltis, L.D.; Bugg, T.D.H. Breaking down lignin to high-value chemicals: The conversion of lignocellulose to vanillin in a gene deletion mutant of *Rhodococcusjostii* RHA1. *ACS Chem. Biol.* **2013**, *8*, 2151–2156. [[CrossRef](#)]
4. Ciriminna, R.; Fidalgo, A.; Meneguzzo, F.; Parrino, F.; Ilharco, L.M.; Pagliaro, M. Vanillin: The case for greener production driven by sustainability megatrend. *ChemPubSoc Eur.* **2019**, *8*, 660–667. [[CrossRef](#)]
5. Fache, M.; Boutevin, B.; Caillol, S. Vanillin production from lignin and its use as a renewable chemical. *ACS Sustain. Chem. Eng.* **2016**, *4*, 35–46. [[CrossRef](#)]
6. Mao, H.-F.; Wang, L.-Z.; Zhao, F.-F.; Wu, J.-X.; Huo, H.-H.; Yu, J. Cobalt-catalyzed aerobic oxidation of eugenol to vanillin and vanillic acid. *J. Chin. Chem. Soc.* **2016**, *63*, 261–266. [[CrossRef](#)]
7. Zhang, R.; Maltari, R.; Guo, M.; Kontro, J.; Eronen, A.; Repo, T. Facile synthesis of vanillin from fractionated Kraft lignin. *Ind. Crops. Prod.* **2020**, *145*, 112095. [[CrossRef](#)]
8. Yamada, M.; Okada, Y.; Yoshida, T.; Nagasawa, T. Biotransformation of isoeugenol to vanillin by *Pseudomonas putida* IE27 cells. *Appl. Microbiol. Biotechnol.* **2007**, *73*, 1025–1030. [[CrossRef](#)]
9. Ashengroph, M.; Nahvi, I.; Zarkesh-Esfahani, H.; Momenbeik, F. *Pseudomonas resinovorans* SPR1, a newly isolated strain with potential of transforming eugenol to vanillin and vanillic acid. *New Biotechnol.* **2011**, *28*, 656–664. [[CrossRef](#)]
10. Kaur, B.; Chakraborty, D. Statistical media and process optimization for biotransformation of rice bran to vanillin using *Pediococcus acidilactici*. *India J. Exp. Biol.* **2013**, *51*, 935–943.
11. Suresh, B.; Ravishankar, G.A. Methyl jasmonate modulated biotransformation of phenylpropanoids to vanillin related metabolites using *Capsicum frutescens* root cultures. *Plant Physiol. Biochem.* **2005**, *43*, 125–131. [[CrossRef](#)]
12. Yamada, M.; Okada, Y.; Yoshida, T.; Nagasawa, T. Vanillin production using *Escherichia coli* cells over-expressing isoeugenol monooxygenase of *Pseudomonas putida*. *Biotechnol. Lett.* **2008**, *30*, 665–670. [[CrossRef](#)]
13. Furuya, T.; Miura, M.; Kuroiwa, M.; Kino, K. High-yield production of vanillin from ferulic acid by a coenzyme-independent decarboxylase/oxygenase two-stage process. *New Biotechnol.* **2015**, *32*, 335–339. [[CrossRef](#)] [[PubMed](#)]
14. Chakraborty, D.; Selvam, A.; Kaur, B.; Wong, J.W.C.; Karthikeyan, O.P. Application of recombinant *Pediococcus acidilactici* BD16 (*fcs*⁺/*ech*⁺) for bioconversion of agrowaste to vanillin. *Appl. Microbiol. Biotechnol.* **2017**, *101*, 5615–5626. [[CrossRef](#)] [[PubMed](#)]
15. Zhao, L.-Q.; Xie, Y.-M.; Chen, L.-Y.; Xu, X.-F.; Zhao, C.X.-X.; Cheng, F. Efficient biotransformation of isoeugenol to vanillin in recombinant strains of *Escherichia coli* by using engineered isoeugenol monooxygenase and sol-gel chitosan membrane. *Process. Biochem.* **2018**, *71*, 76–81. [[CrossRef](#)]
16. Singh, P.; Khan, S.; Pandey, S.; Singh, M.; Banerjee, S.; Kitamura, Y.; Rahman, L. Vanillin production in metabolically engineered *Beta vulgaris* hairy roots through heterologous expression in *Pseudomonas fluorescens* HCHL gene. *Ind. Crops. Prod.* **2015**, *74*, 839–848. [[CrossRef](#)]
17. Paz, A.; Outeiriño, D.; Oliveira, R.P.D.S.; Domínguez, J.M. Fed-batch production of vanillin by *Bacillus aryabhattai* BA03. *New Biotechnol.* **2018**, *40*, 186–191. [[CrossRef](#)] [[PubMed](#)]
18. Kaur, B.; Chakraborty, D.; Kumar, B. Metabolic engineering of *Pediococcus acidilactici* BD16 for production of vanillin through ferulic acid catabolic pathway and process optimization using response surface methodology. *Appl. Microbiol. Biotechnol.* **2014**, *98*, 8539–8551. [[CrossRef](#)]
19. García-Bofill, M.; Sutton, P.W.; Guillén, M.; Álvaro, G. Enzymatic synthesis of vanillin catalyzed by an eugenol oxidase. *Appl. Catal. A-Gen.* **2019**, *582*, 117117.
20. Yamada, M.; Okada, Y.; Yoshida, T.; Nagasawa, T. Purification, characterization and gene cloning of isoeugenol-degrading enzyme from *Pseudomonas putida* IE27. *Arch. Microbiol.* **2007**, *187*, 511–517. [[CrossRef](#)]
21. Ryu, J.Y.; Seo, J.; Park, S.; Ahn, J.H.; Chong, Y.; Sadowsky, M.; Hur, H.G. Characterization of an isoeugenol monooxygenase (Iem) from *Pseudomonas nitroreducens* Jin1 that transforms isoeugenol to vanillin. *Biosci. Biotech. Biochem.* **2013**, *77*, 289–294. [[CrossRef](#)] [[PubMed](#)]

22. Wang, Q.; Wu, X.-M.; Lu, X.-Y.; He, Y.-C.; Ma, B.-D.; Xu, Y. Efficient biosynthesis of vanillin from isoeugenol by recombinant isoeugenol monooxygenase from *Pseudomonas nitroreducens* Jin1. *Appl. Biochem. Biotechnol.* **2021**, *193*, 1116–1128. [[CrossRef](#)] [[PubMed](#)]
23. Porter, J.L.; Rusli, R.A.; Ollis, D.L. Directed evolution of enzymes for industrial biocatalysis. *ChemBioChem* **2016**, *17*, 197–203. [[CrossRef](#)]
24. Tu, T.; Wang, Y.; Huang, H.-Q.; Wang, Y.; Jiang, X.; Wang, Z.-X.; Yao, B.; Luo, H.-Y. Improving the thermostability and catalytic efficiency of glucose oxidase from *Aspergillus niger* by molecular evolution. *Food Chem.* **2019**, *281*, 163–170. [[CrossRef](#)] [[PubMed](#)]
25. Chen, C.; Su, L.-Q.; Xu, F.; Xia, Y.-M.; Wu, J. Improved thermostability of maltooligosyltrehalose synthase from *Arthrobacter ramosus* by directed evolution and site-directed mutagenesis. *J. Agric. Food Chem.* **2019**, *67*, 5587–5595. [[CrossRef](#)]
26. Schmidt, S.; Genz, M.; Balke, K.; Bornscheuer, U.T. The effect of disulfide bond introduction and related Cys/Ser mutations on the stability of a cyclohexanone monooxygenase. *J. Biotechnol.* **2015**, *214*, 199–211. [[CrossRef](#)] [[PubMed](#)]
27. Saab-Rincon, G.; Alwaseem, H.; Guzmán-Luna, V.; Olvera, L.; Fasan, R. Stabilization of the reductase domain in the catalytically self-sufficient cytochrome P450BM3 via consensus-guided mutagenesis. *ChemBioChem* **2018**, *19*, 622–632. [[CrossRef](#)]
28. Hua, Y.-J.; Lyu, C.-J.; Liu, C.-Y.; Wang, H.-P.; Hu, S.; Zhao, W.-R.; Mei, J.-Q.; Huang, J.; Mei, L.-H. Improving the thermostability of glutamate decarboxylase from *Lactobacillus brevis* by consensus mutagenesis. *Appl. Biochem. Biotechnol.* **2020**, *191*, 1456–1469. [[CrossRef](#)]
29. Xie, D.-F.; Yang, J.-X.; Lv, C.-J.; Mei, J.-Q.; Wang, H.-P.; Hu, S.; Zhao, W.-R.; Cao, J.-R.; Tu, J.-L.; Huang, J.; et al. Construction of stabilized (R)-selective amine transaminase from *Aspergillus terreus* by consensus mutagenesis. *J. Biotechnol.* **2019**, *293*, 8–16. [[CrossRef](#)]
30. Wang, R.; Wang, S.; Xu, Y.; Yu, X.-W. Enhancing the thermostability of *Rhizopus chinensis* lipase by rational design and MD simulations. *Int. J. Biol. Macromol.* **2020**, *160*, 1189–1200. [[CrossRef](#)]
31. Argos, P.; Rossmann, M.G.; Grau, U.M.; Zuber, H.; Frank, G.; Tratschin, J.D. Thermal stability and protein structure. *Biochemistry* **1979**, *18*, 5698–5703. [[CrossRef](#)] [[PubMed](#)]
32. Mrabet, N.T.; Van den Broeck, A.; Van den Brande, I.; Stanssens, P.; Laroche, Y.; Lambeir, A.M.; Matthijssens, G.; Jenkins, J.; Chiadmi, M.; Van, T.H. Arginine residues as stabilizing elements in proteins. *Biochemistry* **1992**, *31*, 2239–2253. [[CrossRef](#)]
33. Liu, Z.-M.; Zheng, W.-H.; Wang, C.; Gao, Y.; Cui, W.-J.; Zhou, Z.-M. Characterization of cysteine sulfinic acid decarboxylase from *Tribolium castaneum* and its application in the production of β -alanine. *Appl. Microbiol. Biotechnol.* **2019**, *103*, 9443–9453. [[CrossRef](#)] [[PubMed](#)]
34. Jones, B.J.; Kan, C.N.E.; Luo, C.; Kazlauskas, R.J. Consensus Finder web tool to predict stabilizing substitutions in proteins. *Methods Enzymol.* **2020**, *643*, 129–148.
35. Duan, X.-G.; Chen, J.; Wu, J. Improving the thermostability and catalytic efficiency of *Bacillus deramificans* Pullulanase by site-directed mutagenesis. *Appl. Environ. Microbiol.* **2013**, *79*, 4072–4077. [[CrossRef](#)]
36. Wu, I.; Arnold, F.H. Engineered thermostable fungal Cel6A and Cel7A cellobiohydrolases hydrolyze cellulose efficiently at elevated temperatures. *Biotechnol. Bioeng.* **2013**, *110*, 1874–1883. [[CrossRef](#)]
37. Han, N.-Y.; Ma, Y.; Mu, Y.-L.; Tang, X.-H.; Li, J.-J.; Huang, Z.-X. Enhancing thermal tolerance of a fungal GH11 xylanase guided by B-factor analysis and multiple sequence alignment. *Enzyme Microb. Technol.* **2019**, *131*, 109422. [[CrossRef](#)] [[PubMed](#)]
38. Fraczkiewicz, R.; Braun, W. Exact and efficient analytical calculation of the accessible surface areas and their gradients for macromolecules. *J. Comput. Chem.* **1998**, *19*, 319–333. [[CrossRef](#)]
39. Jones, B.J.; Kan, C.N.E.; Luo, C.; Kazlauskas, R.J. Comparison of five protein engineering strategies to stabilize an α/β -hydrolase. *Biochemistry* **2017**, *56*, 6521–6532. [[CrossRef](#)]
40. Eijnsink, V.; Bjork, A.; Gaseidnes, S.; Sirevag, R.; Synstad, B.; Burg, B.; Vriend, G. Rational engineering of enzyme stability. *J. Biotechnol.* **2004**, *113*, 105–120. [[CrossRef](#)]
41. Li, W.-F.; Zhou, X.-X.; Lu, P. Structural features of thermozymes. *Biotechnol. Adv.* **2005**, *23*, 271–281. [[CrossRef](#)]
42. Mahadevi, A.S.; Sastry, G.N. Cation- π Interaction: Its role and relevance in chemistry, biology and material science. *Chem. Rev.* **2013**, *113*, 2100–2138. [[CrossRef](#)]
43. Kabsch, W.; Sander, C. Dictionary of protein secondary structure: Pattern of hydrogen-bonded and geometrical features. *Biopolymers* **1983**, *22*, 2577–2637. [[CrossRef](#)]
44. Polizzi, K.M.; Bommarius, A.S.; Broering, J.M.; Chaparro-Riggers, J.F. Stability of biocatalysts. *Curr. Opin. Chem. Biol.* **2007**, *11*, 220–225. [[CrossRef](#)]
45. Ashengroph, M.; Nahvi, I.; Zarkesh-Esfahani, H.; Momenbeik, F. *Candida galli* strains PGO6: A novel isolated yeast strain capable of transformation of isoeugenol to vanillin and vanillic acid. *Curr. Microbiol.* **2011**, *62*, 990–998. [[CrossRef](#)]
46. Ashengroph, M.; Nahvi, I.; Zarkesh-Esfahani, H.; Momenbeik, F. Use of growing cells of *Pseudomonas aeruginosa* for synthesis of the natural vanillin via conversion of isoeugenol. *Iran. J. Pharm. Res.* **2011**, *10*, 749–757.
47. Li, Y.-H.; Sun, Z.-H.; Zhao, L.-Q.; Xu, Y. Bioconversion of isoeugenol into vanillin by crude enzyme extracted from soybean. *Appl. Biochem. Biotechnol.* **2005**, *125*, 1–10. [[CrossRef](#)]
48. Arnold, K.; Bordoli, L.; Kopp, J.; Schwede, T. The SWISS-MODEL workspace: A web-based environment for protein structure homology modeling. *Bioinformatics* **2006**, *22*, 195–201. [[CrossRef](#)] [[PubMed](#)]
49. Loewen, P.C.; Switala, J.; Wells, J.P.; Huang, F.; Zara, A.T.; Allingham, J.S.; Loewen, M.C. Structure and function of a lignostilbene- α,β -dioxygenase orthologue from *Pseudomonas brassicacearum*. *BMC Biochem.* **2018**, *19*, 8. [[CrossRef](#)] [[PubMed](#)]

50. Laskowski, R.A.; Jabłońska, J.; Pravda, L.; Vařeková, R.S.; Thornton, J.M. PDBsum: Structural summaries of PDB entries. *Protein Sci.* **2018**, *27*, 129–134. [[CrossRef](#)] [[PubMed](#)]
51. Bowie, J.U.; Lüthy, R.; Eisenberg, D. A method to identify protein sequences that fold into a known three-dimensional structure. *Science* **1991**, *253*, 164–170. [[CrossRef](#)]
52. Larkin, M.A.; Blackshields, G.; Brown, N.P.; Chenna, R.; Mcgettigan, P.A.; Mcwilliam, H.; Valentin, F.; Wallace, I.M.; Wilm, A.; Lopez, R. Clustal W and Clustal X version 2.0. *Bioinformatics* **2007**, *23*, 2947–2948. [[CrossRef](#)]
53. Crooks, G.E.; Hon, G.; Chandonia, J.M.; Brenner, S.E. WebLogo: A sequence logo generator. *Genome Res.* **2004**, *14*, 1188–1190. [[CrossRef](#)] [[PubMed](#)]
54. Ho, S.N.; Hunt, H.D.; Horton, R.M.; Pullen, J.K.; Pease, L.R. Site-directed mutagenesis by overlap extension using the polymerase chain reaction. *Gene* **1989**, *77*, 51–59. [[CrossRef](#)]
55. Bradford, M.M. A rapid and sensitive method for the quantitation of microgram quantities of protein utilizing the principle of protein-dye binding. *Anal. Biochem.* **1976**, *72*, 248–254. [[CrossRef](#)]